

Radiation-Hydrodynamics of Hot Jupiter Atmospheres

Kristen Menou & Emily Rauscher

*Department of Astronomy, Columbia University,
550 West 120th Street, New York, NY 10027, USA*

ABSTRACT

Radiative transfer in planetary atmospheres is usually treated in the static limit, i.e., neglecting atmospheric motions. We argue that hot Jupiter atmospheres, with possibly fast (sonic) wind speeds, may require a more strongly coupled treatment, formally in the regime of radiation-hydrodynamics. To lowest order in v/c , relativistic Doppler shifts distort line profiles along optical paths with finite wind velocity gradients. This leads to flow-dependent deviations in the effective emission and absorption properties of the atmospheric medium. Evaluating the overall impact of these distortions on the radiative structure of a dynamic atmosphere is non-trivial. We present transmissivity and systematic equivalent width excess calculations which suggest possibly important consequences for radiation transport in hot Jupiter atmospheres. If winds are fast and bulk Doppler shifts are indeed important for the global radiative balance, accurate modeling and reliable data interpretation for hot Jupiter atmospheres may prove challenging: it would involve anisotropic and dynamic radiative transfer in a coupled radiation-hydrodynamical flow. On the bright side, it would also imply that the emergent properties of hot Jupiter atmospheres are more direct tracers of their atmospheric flows than is the case for Solar System planets. Radiation-hydrodynamics may also influence radiative transfer in other classes of hot exoplanetary atmospheres with fast winds.

Subject headings: planetary systems, radiative transfer

1. Introduction

In recent years, it has become possible to remotely observe the atmospheres of some exoplanets found in close-in orbits around nearby stars. Many of these observations, which include eclipse, phase curve, and transit photometric or spectroscopic measurements, have focused on the specific class of exoplanets known as hot Jupiters (Charbonneau et al. 2002, 2005; Deming et al. 2005; Charbonneau et al. 2008; Knutson et al. 2008, 2009b; Harrington et al.

2006, 2007; Agol et al. 2009; Cowan et al. 2007; Knutson et al. 2007, 2009a; Tinetti et al. 2007; Pont et al. 2008; Sing et al. 2008; Swain et al. 2008a,b; Grillmair et al. 2007; Richardson et al. 2007). These gaseous giant planets have high atmospheric temperatures, from the close proximity to their parent stars, slow spin rotation rates, as inferred from their expected state of tidal synchronization, and they are thus subject to an unusual steady pattern of hemispheric insolation, with permanent day and night sides (e.g., Seager et al. 2005; Showman et al. 2008b, 2010).

A variety of diagnostics about physical conditions in the atmospheres of a few specific hot Jupiters have been presented in the literature, from the presence of high altitude haze (e.g., Pont et al. 2008) to the existence of vertical temperature inversions (“stratospheres”, e.g., Burrows et al. 2008; Fortney et al. 2008), as well as constraints on the chemical abundances of radiatively active species (e.g., Charbonneau et al. 2002; Tinetti et al. 2007; Sing et al. 2008; Swain et al. 2008b). In most cases, these interpretations rely on one-dimensional, steady-state radiative transfer models describing in great detail the atmospheric structure that is expected at radiative and chemical equilibrium. On the other hand, these models usually consider only globally averaged atmospheric properties and they often ignore the role of horizontal heat transport by advection on the energetic balance of the modeled atmospheres. Such shortcomings of radiative transfer models could eventually limit our ability to reliably infer the physical conditions present in remotely observed exoplanetary atmospheres.

Planetary atmospheres which satisfy global radiative equilibrium are generally not in local radiative equilibrium, that is along a specific vertical column, because of finite contributions from horizontal heat fluxes. The role of atmospheric circulation in shaping the structure and properties of hot Jupiter atmospheres has been recognized as an increasingly important ingredient over the last few years (e.g., Fortney et al. 2006) and several groups have been developing multi-dimensional atmospheric models to address this issue more explicitly (Showman & Guillot 2002; Cho et al. 2003, 2008; Burkert et al. 2005; Cooper & Showman 2005, 2006; Langton & Laughlin 2007; Dobbs-Dixon & Lin 2008; Showman et al. 2008a, 2009; Menou & Rauscher 2009; Rauscher & Menou 2009).

Even in a three-dimensional, time-dependent atmospheric model of the type known as “General Circulation Model” (GCM), radiative transfer is traditionally treated in the static approximation. In this limit, the coupling between the atmospheric flow and the radiative heat transport enters only via the energy equation for the moving atmospheric fluid, so that this coupling is purely thermodynamic in nature. The radiative transfer component of the problem, which is needed to continuously evaluate the net diabatic heating or cooling rate of the gas in motion, is solved independently of the atmospheric motions themselves, as if the atmosphere were actually static.

Here, we argue that this level of thermodynamic coupling, which is a standard approximation for Solar System planetary atmospheres, may be insufficient to describe accurately the nature of energy transport in hot Jupiter atmospheres. A more strongly coupled treatment known as radiation-hydrodynamics, in which flow velocities enter the radiation transport problem explicitly, may be required to describe radiative transfer in hot Jupiter atmospheres with fast, sonic or transonic wind speeds.

The remainder of this paper is organized as follows. In §2, we outline the general formalism for radiation transport in a dynamic atmosphere. We motivate the relevance of this radiation-hydrodynamics regime for hot Jupiter atmospheres with fast winds in §3. We discuss the potential magnitude of deviations from the static limit for the global radiative balance of hot Jupiter atmospheres in §4 and we conclude in §5.

2. Radiative Transfer in Dynamic Atmospheres

Radiation-hydrodynamics requires a fully relativistic treatment to properly account for Doppler shifts and aberration effects (Mihalas & Mihalas 1984; Castor 2004). The time-dependent radiation transport equation in the fluid comoving frame, to leading order in the ratio of the fluid velocity to the speed of light, v/c , was derived by Buchler (1983, see also Hsieh & Spiegel 1976). The breakdown of terms in this rather general equation, which may or may not be discarded depending on the nature of the physical problem at hand, is a delicate matter (Castor 2004; Mihalas & Mihalas 1984). In the limit of slow fluid motions ($v/c \ll 1$) and thus fast light-transit times, however, there is general agreement that the leading order effect of fluid motions is simply to induce Doppler shifts in the instantaneous radiation field seen by the fluid (e.g., Rybicki 1970; Rybicki & Hummer 1978).¹ This results in modified absorption and emission coefficients for radiation-matter interaction, particularly when these interactions are dominated by line opacities. In the remainder of this work, we focus our discussion on line opacities, which are expected to dominate in hot Jupiter atmospheres, and neglect continuum sources of opacities.

Much of the astrophysical literature on radiation-hydrodynamics is focused on the radiative transfer of radially expanding stellar winds. We start our discussion closely following the formalism of Rybicki & Hummer (1978). To lowest order in v/c , the radiative transfer equation in a moving medium can be written

¹Effects due to relativistic aberration are thought to be significant only at higher order in v/c (Castor 2004).

$$\mathbf{n} \cdot \nabla I(\mathbf{r}, \mathbf{n}, \nu) = -k_{\text{tot}}(\mathbf{r}) \Phi \left[(\nu - \nu_0) + \frac{\nu_0}{c} \mathbf{n} \cdot \mathbf{v}(\mathbf{r}) \right] [I(\mathbf{r}, \mathbf{n}, \nu) - S(\mathbf{r}, \mathbf{n}, \nu)], \quad (1)$$

where $I(\mathbf{r}, \mathbf{n}, \nu)$ is the monochromatic intensity (per unit solid angle) at frequency ν and spatial location \mathbf{r} in the direction defined by the unit vector \mathbf{n} , S is the source function, $\mathbf{v}(\mathbf{r})$ is the material velocity field, k_{tot} is the line integrated opacity, ν_0 is the line central frequency and $\Phi(\nu)$ is the line profile function, normalized to unity. The standard radiative transfer equation in the static limit is recovered by forcing $\mathbf{v}(\mathbf{r})$ to zero.

Equation (1) expresses the fact that any projected velocity gradient along an optical path in the direction \mathbf{n} leads to a shift in the line profile, and thus a change in the effective absorption coefficient of the medium, in proportion to the Doppler term $\mathbf{n} \cdot \mathbf{v}(\mathbf{r})\nu_0/c$ entering the line function Φ . By contrast, a uniform velocity field leads to a more trivial, uniform frequency shift. In the context of stellar wind theory, equation (1) is typically solved using the approximate ‘‘Sobolev method,’’ in the limit of strongly supersonic gradient flow motions, for radially expanding shells of material (e.g., Rybicki & Hummer 1978; Castor 2004). This is not the limit of interest for hot Jupiter atmospheres.

The literature on radiative transfer in static atmospheres is vast and the reader is directed to the monographs by Goody & Yung (1989), Thomas & Stamnes (2002) and Liou (2002) for detailed accounts on this subject. To make the connection with that work, we now introduce the plane-parallel atmosphere approximation, using z as the vertical coordinate in the atmosphere. In addition, we introduce the zenith angle θ (away from the vertical axis, pointing upward) and the azimuthal angle ϕ (in the plane normal to the vertical). It is convenient to introduce the quantity $\mu = \cos \theta$, which ranges from +1 going up to -1 going down in the plane-parallel atmosphere. We further assume that local thermodynamic equilibrium is satisfied and we neglect scattering, as is generally justified for the thermal portion of the atmospheric radiation spectrum.² The source function S then reduces to the Planck function, $B_\nu(T(z)) = B_\nu(z)$. In that case, the formal solution to the radiative transfer equation for the monochromatic intensity at level z_0 in the direction (μ, ϕ) can be written (Goody & Yung 1989; Thomas & Stamnes 2002; Liou 2002):

²It is customary in the treatment of atmospheric radiation to separate the short-wavelength component of the spectrum, which is related to beam-like insolation in the presence of scattering (typically in the optical), from the long-wavelength component, which is related to diffuse thermal emission from the various atmospheric layers (typically in the infrared). We follow this convention here, even though the two spectral components are not as clearly separated for hot Jupiters as they are for ‘‘cool’’ Solar System planets. For simplicity, we focus our entire discussion on the long-wavelength thermal component and postpone a discussion of possible complications with the short-wavelength portion of the radiation spectrum until §5.

$$I_\nu(z_0; \mu, \phi) = I_\nu(0; \mu, \phi)\mathcal{T}_\nu(0, z_0; \mu, \phi) + \int_0^{z_0} B_\nu(z; \mu, \phi) \frac{d\mathcal{T}_\nu(z, z_0; \mu, \phi)}{dz} dz, \quad (2)$$

where the monochromatic notation has been changed to I_ν and $z = 0$ corresponds to a bounding region for the atmosphere (e.g., the bulk interior), with a one-sided radiative boundary condition specified as $I_\nu(0; \mu, \phi)$. The first term on the RHS of eq. (2) describes the cumulative absorption of $I_\nu(0; \mu, \phi)$ from $z = 0$ to z_0 along the optical path, while the second term describes the cumulative Planck emission, and its absorption, integrated over all layers along the optical path, from $z = 0$ to z_0 . The monochromatic transmissivity

$$\mathcal{T}_\nu(z, z_0; \mu, \phi) \equiv \exp \left[- \int_z^{z_0} k_\nu(z'; \mu, \phi) \rho(z'; \mu, \phi) dz' \right] \quad (3)$$

encapsulates the absorption (and emission) properties of the medium. It is the integral of the mass absorption coefficient k_ν weighted by the amount of absorber (with mass density ρ), between vertical levels z and z_0 , along the optical path defined by the direction (μ, ϕ) .

According to equation (1), bulk Doppler shifts in a dynamic atmosphere modify the radiative transfer by changing the monochromatic absorption coefficient (unit of cross section per unit mass),

$$k_\nu(z'; \mu, \phi) = k_{\text{tot}}(\mathbf{r}) \Phi \left[(\nu - \nu_0) + \frac{\nu_0}{c} \mathbf{n} \cdot \mathbf{v}(\mathbf{r}) \right], \quad (4)$$

or equivalently by changing the monochromatic transmissivities, $\mathcal{T}_\nu(z, z_0; \mu, \phi)$, in equation (2). If bulk Doppler shifts are important and the material velocity field is anisotropic, so is the radiative transfer.

By property of isotropy of the Planck source function, a large fraction of the thermal atmospheric radiation field is carried along rays which are significantly slanted relative to the vertical, even though net flux exchange between atmospheric layers occurs vertically. The next step in deriving vertical flux equations for the atmospheric radiation problem typically involves separate angular integrations for the ascending ($\mu > 0$) and descending ($\mu < 0$) fluxes (Goody & Yung 1989; Thomas & Stamnes 2002; Liou 2002), of the type

$$F_\nu^\pm = \int_0^{2\pi} \int_0^{\pm 1} I_\nu(\mu, \phi) \mu d\mu d\phi. \quad (5)$$

To account for the phase space available at slanted angles, it is customary in “two-stream” formulations to replace all angular integrals over transmissivities by a single average transmissivity value for a characteristic zenith angle, $\mu_0 = \cos \theta_0$:

$$\int_0^{2\pi} \int_0^{\pm 1} \exp \left[- \int_z^{z_0} k_\nu(z'; \mu, \phi) \rho(z'; \mu, \phi) dz' \right] \mu d\mu d\phi$$

$$\simeq \pi \exp \left[- \frac{1}{\mu_0} \int_z^{z_0} k_\nu(z'; \mu_0) \rho(z'; \mu_0) dz' \right] \equiv \bar{\mathcal{T}}_\nu(z, z_0), \quad (6)$$

where $\bar{\mathcal{T}}_\nu$ is the hemispherically-averaged “diffusive transmissivity.” This approximation has been shown to yield errors $\lesssim 1.5\%$ in typical applications for static atmospheres, when a diffusivity factor $1/\mu_0 = 1.66$ is adopted (Rodgers & Walshaw 1966; Goody & Yung 1989; Thomas & Stamnes 2002; Liou 2002), which corresponds to a zenith angle $\theta_0 = 53$ deg. This relatively large value of the effective zenith angle illustrates well the large phase space available for thermal radiation at slanted angles. It indicates that the projected wind velocity along a typical optical path for thermal atmospheric radiation can be a significant fraction of the full horizontal wind speed,³ even though net radiative exchanges between the atmospheric layers occur in the vertical.

3. Hot Jupiter Atmospheres

To help us focus our discussion further, we now turn to issues specific to hot Jupiter atmospheres.

3.1. Projected Wind Velocities

Over the last few years, various circulation models have indicated that wind speeds could reach sonic or even supersonic values in the upper atmospheres of hot Jupiters (Cooper & Showman 2005, 2006; Dobbs-Dixon & Lin 2008; Showman et al. 2008a, 2009; Rauscher & Menou 2009). Here, for concreteness, we use the specific hot Jupiter model described in Rauscher & Menou (2009) to evaluate the magnitude of projected velocity gradients along representative optical paths for thermal radiation in a dynamic hot Jupiter atmosphere.

A specific optical path is defined by a starting location at the bottom of the model atmosphere and by a unit vector \mathbf{n} which defines the path orientation. We calculate the projected wind velocity along this path throughout the entire model atmosphere as

³Large scale motions are predominantly horizontal in an atmosphere.

$$V_{\text{proj}} = \mathbf{n} \cdot \mathbf{V}_{\mathbf{h}} = \mathbf{n}_{\mathbf{h}} \cdot \mathbf{V}_{\mathbf{h}} \sin \theta_0, \quad (7)$$

where $\mathbf{V}_{\mathbf{h}}$ is the wind horizontal velocity vector according to the circulation model, $\mathbf{n}_{\mathbf{h}}$ is the horizontal unit vector projected on the sphere (i.e., defining the north/south and east/west directions) and the representative zenith angle $\theta_0 = 53$ deg is uniformly adopted in all our calculations. A detailed calculation would require us to take into account the three-dimensional geometry of the problem, with varying pressure levels in each of the model vertical columns crossed by the slanted optical path. Rather than performing delicate three-dimensional interpolations between various model columns, we use the profile of wind velocities in a single vertical column. That is, we use values of $\mathbf{V}_{\mathbf{h}}$ as if the optical path were exactly vertical, even though the calculation assumes a zenith angle $\theta_0 = 53$ deg and various azimuthal orientations for the projection. While this approximation clearly emphasizes vertical velocity gradients over horizontal ones, it still captures representative changes in $\mathbf{V}_{\mathbf{h}}$, both in magnitude and direction, along the selected optical path (with a specific azimuthal orientation). It should thus be sufficient to evaluate the typical magnitude of projected velocity gradients along representative optical paths in the model atmosphere.

Figure 1 shows profiles of wind velocity projected along representative optical paths, as a function of pressure, p (a proxy for height in the atmosphere). All velocities are expressed in units of the local value of the adiabatic sound speed, $V_{\text{proj}}(p)/c_s(p; T)$. The same H_2 -dominated atmospheric gas parameters as in Rauscher & Menou (2009) are used to calculate the sound speed: $c_s \equiv \sqrt{\gamma \mathcal{R} T}$, with an adiabatic index $\gamma = 1/(1 - \kappa)$, $\kappa = 0.321$ and a gas constant $\mathcal{R} = 4593 \text{ J kg}^{-1} \text{ K}^{-1}$. The various panels show profiles at the model substellar point (a), antistellar point (b), west equatorial terminator (c) and north pole (d). In each panel, the various curves show projected velocity profiles for optical paths oriented to the east (solid line), north-east (dotted), north (dashed) and north-west (dash-dotted) on the sphere. Projected velocity profiles for other cardinal directions can be deduced by symmetry.

Figure 1 reveals significant gradients in projected wind velocity as one crosses the atmosphere along representative slanted optical paths for thermal radiation. Velocity differentials over one pressure scale height easily amount to ~ 0.2 - $0.5 c_s$ and they exceed c_s in some cases, especially high up in the atmosphere. Velocity differentials $\gtrsim c_s$ are typical when crossing several pressure scale heights.

The different panels in Figure 1 illustrate the diverse character of projected velocity profiles at various locations around the planet. Furthermore, panels a), b) and c) exemplify the anisotropic nature of these projected velocity profiles. Projected velocity gradients are systematically weak in the north (or equivalently south) direction but they can become significant when the east-west direction is sufficiently sampled by the optical path

under consideration. This is easily understood as resulting from the predominantly zonal (east-west) nature of winds in this and other hot Jupiter atmospheric circulation models (Rauscher & Menou 2009; Showman et al. 2008b). It is then clear that the azimuthal angular phase space for thermal radiation will be dominated by optical paths sampling significant velocity gradients, with unusually low gradient values relevant only for the small fraction of all paths that are closely aligned with the north-south direction. As discussed in §2, to the extent that projected velocity gradients of the magnitude shown in Fig. 1 impact the transport of thermal radiation, the radiative transfer problem will become anisotropic via the sampling of a variety of azimuthal and zenith angles, even when the Planck source function itself is isotropic (in the fluid frame).

3.2. Line Shapes and Widths

Opacity sources in hot Jupiter atmospheres are largely dominated by discrete atomic and molecular lines, particularly in the thermal portion of the atmospheric radiation spectrum (e.g., Sharp & Burrows 2007; Freedman et al. 2008). Lines are broadened well beyond their quantum mechanical width through Doppler shifts associated with the thermal motions of atomic and molecular constituents (“Doppler broadening”) and through the effect of collisions of these atoms and molecules with other gas constituents (“pressure broadening”). The relative width of Doppler and pressure broadening depends on the local conditions of density and temperature in the atmosphere, as well as on the specific radiative constituent under consideration. The general shape of a line that is both Doppler- and pressure-broadened, i.e. the detailed functional form of the line function Φ in eq. (1), is given by the Voigt function (Goody & Yung 1989; Thomas & Stamnes 2002; Liou 2002).

Intuitively, one expects the radiation transport in an atmosphere with strongly pressure-broadened lines and very subsonic wind speeds to be relatively insensitive to the additional Doppler shifts due to bulk flow velocities projected along various optical paths. Indeed, the typical thermal width of a Doppler-broadened line is closely related to the sound speed of the atmospheric gas (see eq. [10] below), so that bulk line shifts should only minimally deform line shapes in the limit of very subsonic wind speeds. This, combined with the dominance of pressure broadening, is the main justification behind the use of a static treatment for radiation transport in Solar System planetary atmospheres (e.g., Goody & Yung 1989). To evaluate the possible role of bulk Doppler shifts for radiation transport in hot Jupiter atmospheres, it is thus important to evaluate the shapes and widths of radiative lines in these atmospheres.

Various static, globally-averaged radiative transfer studies have established that the ra-

diatively forced regions of hot Jupiter atmospheres are found, broadly speaking, above the 10–100 bar pressure level (e.g., Seager & Sasselov 1998; Sudarsky et al. 2000; Barman et al. 2005; Iro et al. 2005; Seager et al. 2005). These models also indicate that photospheric levels⁴ vary strongly with wavelength in the optical–IR spectral range, as a result of strong variations in line opacities, from a few bars to $\lesssim 10^{-2}$ bars typically (e.g., Seager et al. 2005; Sharp & Burrows 2007). Regions in the pressure range from ~ 10 to 10^{-3} bars are thus of particular interest for the study of radiation transport in dynamic hot Jupiter atmospheres.

A detailed account of the typical treatment of lines in static radiative transfer calculations for hot Jupiter atmospheres is provided by Sharp & Burrows (2007). The general Voigt profile of a pressure- and Doppler-broadened line is given by

$$\Phi_V(\nu - \nu_0) = \frac{1}{\pi^{3/2}} \frac{\Delta\nu_p}{\Delta\nu_D} \int_{-\infty}^{+\infty} \frac{1}{(\nu' - \nu_0)^2 + \Delta\nu_p^2} \exp\left[-\frac{(\nu - \nu')^2}{\Delta\nu_D^2}\right] d\nu', \quad (8)$$

where $\Delta\nu_p$ and $\Delta\nu_D$ measure the pressure and Doppler broadening widths, respectively, and Φ_V is normalized to unity (Goody & Yung 1989; Thomas & Stamnes 2002; Liou 2002). Pressure broadening generally depends on pressure, temperature and the radiative constituent under consideration but the “classical” scaling

$$\Delta\nu_p = 0.02 - 0.05 \left(\frac{P}{1 \text{ bar}}\right) \left(\frac{T}{1500 \text{ K}}\right)^{-1/2} \text{ cm}^{-1}, \quad (9)$$

with a $-1/2$ power law dependence on temperature, should be sufficient for our order-of-magnitude estimates (Goody & Yung 1989; Thomas & Stamnes 2002; Liou 2002; Sharp & Burrows 2007). Doppler broadening depends on temperature, wavelength ($\lambda_0 = c/\nu_0$) and the mass, m_{mol} , of the radiative constituent under consideration,

$$\Delta\nu_D \equiv \frac{\nu_0}{c} \sqrt{\frac{2kT}{m_{\text{mol}}}} \simeq \frac{\nu_0}{c} \sqrt{\frac{2m_{\text{H}_2}}{\gamma m_{\text{mol}}}} c_s \simeq 0.14 \left(\frac{m_{\text{H}_2}}{m_{\text{mol}}}\right)^{1/2} \left(\frac{T}{1500 \text{ K}}\right)^{1/2} \left(\frac{\lambda_0}{1 \text{ }\mu\text{m}}\right)^{-1} \text{ cm}^{-1}, \quad (10)$$

where m_{H_2} is the mass of the H_2 molecule (the dominant atmospheric constituent), γ is the gas adiabatic index and c_s is the corresponding adiabatic sound speed. This scaling illustrates how the Doppler width is reduced for radiative constituents which are typically more massive than molecular hydrogen. Note that the linear scaling of $\Delta\nu_D$ with the central

⁴The photosphere can be defined as the height in the atmosphere at which photon escape to space becomes possible, i.e., where the monochromatic optical thickness approaches unity.

wavelength λ_0 implies significant Doppler width variations across the relevant optical-IR spectral range.

Substantial variations in temperature on constant pressure levels are found, from day- to night-side, in current atmospheric circulation models for hot Jupiters (Cooper & Showman 2005, 2006; Langton & Laughlin 2007; Dobbs-Dixon & Lin 2008; Showman et al. 2008a, 2009; Menou & Rauscher 2009; Rauscher & Menou 2009). Here, for simplicity, we choose $T = 1500$ K and 1000 K as representative temperature values at the 1 bar and 10^{-2} bar levels, respectively (see, e.g., Fig. 3 of Rauscher & Menou 2009). The ratio of Doppler to pressure broadening widths is given by

$$\frac{\Delta\nu_D}{\Delta\nu_p} = 3 - 7 \left(\frac{m_{\text{H}_2}}{m_{\text{mol}}} \right)^{1/2} \left(\frac{T}{1500 \text{ K}} \right) \left(\frac{P}{1 \text{ bar}} \right)^{-1} \left(\frac{\lambda_0}{1 \mu\text{m}} \right)^{-1}. \quad (11)$$

For relevant molecules, typical values of the mass ratio factor, $(m_{\text{H}_2}/m_{\text{mol}})^{1/2}$, are $\simeq 1/2.8$ (CH_4), $1/3$ (H_2O), $1/4.7$ (CO_2) and $1/5.6$ (TiO). At 1 bar, for $T = 1500$ K, the typical broadening ratio is thus $\Delta\nu_D/\Delta\nu_p \simeq 0.5 - 2$ at $1 \mu\text{m}$ and $0.05 - 0.2$ at $10 \mu\text{m}$. At 10^{-2} bar and $T = 1000$ K, the ratio becomes $\Delta\nu_D/\Delta\nu_p \simeq 30 - 130$ at $1 \mu\text{m}$ and $3 - 13$ at $10 \mu\text{m}$. Doppler broadening is thus significant at the 1 bar level, especially in the near-IR and the optical, and it becomes increasingly dominant across the entire optical-IR spectral range higher up in the atmosphere.

The sizable contribution of thermal Doppler broadening to the width of radiative lines at photospheric levels in hot Jupiter atmospheres, together with the scaling $\Delta\nu_D < c_s \times \nu_0/c$ from Eq. (10), suggests that bulk Doppler shifts from atmospheric motions near the sound speed could modify the shapes of radiative lines significantly. By contrast, much deeper in the atmosphere, where $\Delta\nu_D/\Delta\nu_p \ll 1$, Doppler shifts from bulk atmospheric motions near the sound speed would only amount to small shifts over comparatively wide, pressure-broadened lines. Furthermore, wind speeds themselves may be reduced at these deeper levels (see, e.g., Fig.1).

These qualitative arguments are not very informative about the possible consequences of bulk Doppler shifts on radiation transport in a dynamic atmosphere. In particular, since the Doppler cores of radiative lines are often very optically thick (“saturated”) in hot Jupiter and other planetary atmospheres, they do not necessarily contribute much to the overall atmospheric energy budget, at least in the static case.⁵ To help us evaluate more quantitatively

⁵Although this is not always explicitly stated, line-by-line radiative transfer models for hot Jupiter atmospheres currently available in the literature, with typical spectral resolutions $\sim 1 \text{ cm}^{-1}$ (e.g.,

the magnitude of bulk Doppler shift effects, we now turn to models of line transmissivities and equivalent widths in dynamic atmospheres.

4. Transmissivity and Equivalent Width Models

4.1. Transmissivities

As summarized in §2, monochromatic transmissivities encapsulate the absorption and emission properties of the atmospheric medium (eqs. [2–3]). Here, we isolate the effects of velocity gradients along an arbitrary optical path by modeling the monochromatic transmissivity in a dynamic atmosphere as

$$\mathcal{T}_\nu = \exp \left[- \int_0^1 \tilde{k}_{\text{tot}} \Phi_V \left[(\nu - \nu_0) + \frac{\nu_0}{c} V_{\text{proj}} \times s' \right] ds' \right], \quad (12)$$

where s' is the length along the unit optical path,⁶ the line integrated opacity \tilde{k}_{tot} is assumed to be constant along the path and Φ_V is the dimensionless Voigt line profile defined in Eq. (8). The above expression for the bulk Doppler shift term in the line function assumes a constant velocity gradient along the path, i.e. a velocity offset that increases linearly with s' , from 0 at $s' = 0$ to the maximum value V_{proj} at $s' = 1$. This simple model isolates the effects of bulk Doppler shifts by assuming that the path is otherwise homogeneous. In a more realistic atmospheric model, optical paths would be inhomogeneous, with line strengths, \tilde{k}_{tot} , generally varying with temperature and line shapes, Φ_V , generally varying with both temperature and pressure along the specific path (Goody & Yung 1989; Thomas & Stamnes 2002; Liou 2002).⁷

Sharp & Burrows 2007; Seager & Sasselov 1998; Seager et al. 2005), do not necessarily resolve the narrow Doppler cores of radiative lines, with typical widths $\Delta\nu_D \ll 1 \text{ cm}^{-1}$ according to Eq. (10).

⁶In Eq. (12), \tilde{k}_{tot} has unit of inverse length. Without loss of generality, we only consider optical paths of unit length in our simplified model. As a result, \tilde{k}_{tot} fully characterizes the optical thickness of the modeled path. To differentiate the more general line integrated opacity k_{tot} appearing in Eq (4), which has units of cross-section per unit mass, from the simpler formulation adopted above, we write it as \tilde{k}_{tot} in the simplified model.

⁷In principle, the combination of Eqs. (3), (4) and (8) requires one to account for the profile variation with pressure and temperature separately for each individual line along the optical path of interest. A very common simplifying assumption in the treatment of atmospheric radiation, known as the Curtis-Godson approximation, is to treat the optical path as if it were homogeneous, i.e. with constant pressure and temperature, and use adequately path-averaged values for the line strength, shape and the absorber amount

Figure 2 shows representative profiles of monochromatic transmissivities for a single line centered at $\nu = \nu_0$ in the model described by Eq. (12). Fixed values for the line integrated opacity, $\tilde{k}_{\text{tot}} = 3$, and for the ratio of Doppler to pressure broadening widths, $\Delta\nu_D/\Delta\nu_p = 10$, were adopted. The deepest transmissivity curve corresponds to the static reference model, with $V_{\text{proj}} = 0$. In decreasing order of profile depth, from left to right, the other curves correspond to models with total velocity offsets $V_{\text{proj}} = 1, 3, 5, 7$ and $9 \Delta\nu_D \times c/\nu_0$, i.e., in units of the thermal Doppler width.

From the point of view of absorption, transmissivities $\mathcal{T}_\nu \lesssim 1$ correspond to the minimal absorption of the optically thin regime, while $\mathcal{T}_\nu \ll 1$ correspond to the strong absorption limit of the optically thick regime. As is clear from Figure 2, monochromatic transmissivities can be considerably affected by bulk Doppler shifts approaching or exceeding the thermal Doppler width, $\Delta\nu_D$, of the line under consideration. A switch from partially optically-thick to fully optically thin occurs in Figure 2. While only the case with $\tilde{k}_{\text{tot}} = 3$ is shown, the shift and the flattening of line transmissivities seen here is qualitatively representative of what is seen for more general cases, with values of \tilde{k}_{tot} ranging from $\ll 1$ to $\gg 1$. We note that the flat-top nature of line transmissivities shown in Figure 2 when velocity gradients are large, i.e., $V_{\text{proj}} \gg \Delta\nu_D \times c/\nu_0$, is consistent with the flattening discussed by Castor (1970) using the Sobolev approximation (see his Fig. 4).

It is worth emphasizing that the magnitude of the velocity gradients considered in Figure 2 are relevant to hot Jupiter atmospheres. Writing the bulk Doppler shift term in Equation (1) as $\Delta\nu_{\text{bulk}} = \mathbf{n} \cdot \mathbf{v}(\mathbf{r}) \times \nu_0/c$, we can express its overall magnitude in our simple transmissivity model in terms of the thermal Doppler width, $\Delta\nu_D$, as

$$\frac{\Delta\nu_{\text{bulk}}}{\Delta\nu_D} = \sqrt{\frac{\gamma m_{\text{mol}}}{2m_{\text{H}_2}} \frac{V_{\text{proj}}}{c_s}}. \quad (13)$$

Since, as seen earlier, the square root factor can reach values up to 5–6 for relevant molecules and, as suggested by Figure 1, differentials of projected velocities can reach up to $V_{\text{proj}} \sim 1\text{--}2 c_s$ along some atmospheric optical paths, the entire range of velocity offset values considered in Figure 2 is probably of interest for hot Jupiter atmospheres.

(e.g., Rodgers & Walshaw 1966; Goody & Yung 1989; Thomas & Stamnes 2002; Liou 2002). While the accuracy of the Curtis-Godson approximation has been extensively tested in the context of static atmospheric radiation transport, its possible breakdown when optical paths acquire anisotropic properties in the presence of bulk Doppler shifts could lead to subtle complications in the treatment of radiation transport in a dynamic atmosphere. This specific aspect of the problem is not explicitly addressed by our simple transmissivity models.

By themselves, offsets and distortions of line transmissivities of the type shown in Figure 2 are not observationally too significant because they occur over spectral intervals typically $< 1 \text{ cm}^{-1}$, which is well below the effective resolving power achieved in optical-IR spectroscopic studies of hot Jupiter atmospheres. To the extent that such bulk Doppler distortions can alter the radiative energy balance in the dynamic atmosphere, however, they could in principle modify the radiative structure of hot Jupiter atmospheres. To evaluate the magnitude of this effect, we turn to a discussion of line equivalent widths.

4.2. Equivalent Widths

Let us first justify our use of equivalent widths by borrowing from the existing literature on “narrow-band” spectral models (Goody & Yung 1989; Thomas & Stamnes 2002; Liou 2002). Ignoring the boundary term for simplicity, the integral term for the intensity given in Eq. (2) is essentially of the form

$$I_\nu = \int_0^1 B_\nu d\mathcal{T}_\nu, \quad (14)$$

which is simply reformulating it as the cumulative Planck emission and its absorption along a specific optical path, weighed by the transmissivities of the various contributing layers, from closely adjacent ones (with transmissivity $\mathcal{T}_\nu \simeq 1$) to more distant ones (with $\mathcal{T}_\nu \simeq 0$, in the optically thick limit). In narrow-band models, the frequency-integrated intensity is written

$$I = \int_0^\infty d\nu \int_0^1 B_\nu d\mathcal{T}_\nu \simeq \sum_i \Delta\nu_i \int_0^1 B_i d\bar{\mathcal{T}}_i, \quad (15)$$

where $\Delta\nu_i$ is the frequency span of the i th narrow band, the Planck function value B_i is considered to be a constant over each narrow band and the band-averaged transmissivities are defined by

$$\bar{\mathcal{T}}_i \equiv \frac{1}{\Delta\nu_i} \int_{\Delta\nu_i} \mathcal{T}_\nu d\nu. \quad (16)$$

The narrow-band formalism is well justified as long as the number of narrow bands is sufficiently large for the Planck function to be well approximated by a constant in each band (Goody & Yung 1989; Thomas & Stamnes 2002; Liou 2002). Since atmospheric fluxes are obtained by angular integration of the intensity, equation (15) relates the radiative energy

balance of the atmosphere to multiple Planck-weighted integrals of band-averaged transmissivities.

The narrow-band formalism is traditionally used with bands that are still wide enough to encompass a large number of individual radiative lines. By contrast, we use it here in its simplest formulation, with very narrow bands including only a single spectral line, assuming that each such line is well isolated from all the other lines (see, e.g., Goody & Yung 1989, chapter 4). In that limit, the equivalent width (EW) of a specific line can be written

$$EW = \int_{\Delta\nu_i} (1 - \mathcal{T}_\nu) d\nu = \Delta\nu_i(1 - \bar{\mathcal{T}}_i), \quad (17)$$

where $\Delta\nu_i$ now represents the typical spacing between neighboring isolated lines. It should be noted that the EW is independent of the value of $\Delta\nu_i$ adopted as long as the spectral interval is large enough to encompass all of the transmissivity values contributing meaningfully to the above integral (i.e., $\mathcal{T}_\nu < 1$). Thus, when line overlap can be omitted, Eqs. (15–17) clarify the direct relation that exists between the radiative energy balance of an atmosphere ($\propto I$), Planck-weighted integrals of band-averaged transmissivities ($\propto d\bar{\mathcal{T}}_i$) and the equivalent widths of all important radiative lines ($d\bar{\mathcal{T}}_i \propto -dEW$). This is our main justification for using deviations in line equivalent widths as a quantitative measure of the effects of bulk Doppler shifts on the overall radiative balance of a dynamic atmosphere.

We perform equivalent width calculations by integrating transmissivity profiles like the ones shown in Figure 1, following equation (17). For the calculations presented here, we verified that our EW results are independent of the spectral interval chosen for integration, as long as it spans more than 100–1000 thermal Doppler widths ($\Delta\nu_D$) on each side of the line central frequency, ν_0 . We evaluate the effects of bulk Doppler shifts simply by comparing the equivalent widths of lines in a static atmosphere, $EW_0 = EW(V_{\text{proj}} = 0)$, to those obtained in the presence of finite bulk Doppler shifts ($V_{\text{proj}} \neq 0$).

In all our calculations, using the simple transmissivity model described by Eq. (12), we find that EWs in dynamic atmospheres are systematically larger than the corresponding value in a static atmosphere, EW_0 . We quantify this trend with the fractional excess, $EW/EW_0 - 1$, expressed in percents. For example, for the various shifted transmissivity profiles shown in Figure 2, we find EW excesses of 2.4, 14, 24, 31 and 35% over the static EW_0 value for the profiles with total velocity offsets $V_{\text{proj}} = 1, 3, 5, 7$ and $9 \Delta\nu_D \times c/\nu_0$, respectively.

Figure 3 further clarifies the variation of the EW excess with the magnitude of the total velocity offset, V_{proj} , in units of $\Delta\nu_D \times c/\nu_0$, in a model with fixed ratio of broadening widths, $\Delta\nu_D/\Delta\nu_p = 10$, for the Voigt line function. The various curves show models with

line integrated absorption coefficient $\tilde{k}_{\text{tot}} = 0.3$ (dashed line), 3 (dotted; same as in Fig. 2), 30 (solid), 300 (dash-dotted) and 3000 (triple-dot dashed). While the EW excesses increase with the value of V_{proj} , the exact dependence is not entirely trivial. For $\tilde{k}_{\text{tot}} = 3, 30$ and 300, EW excesses from several tens of percents to more than a hundred percent are possible, for the same range of V_{proj} values as deemed relevant for hot Jupiter atmospheres earlier.

Figure 4 shows the systematic variation of the EW excess with the magnitude of the total line absorption coefficient, \tilde{k}_{tot} , in a model with a value of the total velocity offset fixed at $V_{\text{proj}} = 10 \Delta\nu_D \times c/\nu_0$. The various curves show models with Voigt function broadening ratios $\Delta\nu_D/\Delta\nu_p = 1$ (dashed line), 10 (dotted; same as in Figs. 2 and 3), 100 (solid) and 1000 (dash-dotted). The EW excess first increases with the value of \tilde{k}_{tot} , peaks around $\tilde{k}_{\text{tot}} \sim 20$ -40 and then drops at larger \tilde{k}_{tot} values. Peak EW excesses are thus reached for rather strong optically thick conditions. Note that EW excesses ~ 150 -200% are possible for $\tilde{k}_{\text{tot}} \sim 30$, $\Delta\nu_D/\Delta\nu_p \gtrsim 100$ and $V_{\text{proj}} \sim 10 \Delta\nu_D \times c/\nu_0$. EW excesses easily reach several tens of percents at $\tilde{k}_{\text{tot}} \sim 30$ in all of the models considered here, for the rather large value of $V_{\text{proj}} = 10 \Delta\nu_D \times c/\nu_0$ adopted (see again Fig. 3 for the dependence with V_{proj}).

We can understand various trends in the behavior of the EW excesses with V_{proj} , \tilde{k}_{tot} and $\Delta\nu_D/\Delta\nu_p$ in our simple models as follows. As already mentioned earlier, we have found that the shifts and distortions of monochromatic transmissivity profiles shown in Fig. 2 are qualitatively representative of the general behavior seen in all our models, whether the line is in the optically thin or optically thick regime. For a line well into the optically thick regime ($1 - \mathcal{T}_{\nu_0} \simeq 1$), the growth in EW with V_{proj} can be simply understood as a stretching of the optically thick portion of the transmissivity curve, which contributes maximally to the growth in EW according to the integral in equation (17). This is the main trend observed for moderate to high values of \tilde{k}_{tot} in Figure 3.

In the optically thin regime, the increase in EW excess with \tilde{k}_{tot} can be understood as resulting from the presence of larger radiative intensities outside the line center (where maximum absorption occurs), so that Doppler-shifted absorption around the line center contributes increasingly to the EW excess. As the value of \tilde{k}_{tot} is increased well into the optically thick regime, however, the much shallower pressure-broadened wings of the Voigt line profile start making a significant contribution to the EW integral, over an increasingly wider range of frequencies. This reduces the effective contribution of the optically-thick, shifted Doppler core to the total line EW, which explains the decline in EW excess at large \tilde{k}_{tot} values in Figure 4, the more so in models with larger values of the pressure-broadening parameter, $\Delta\nu_p$.

5. Discussion and Conclusion

Our main result has been to establish the possibility that bulk Doppler shifts from fast, sonic or transonic wind speeds in hot Jupiter atmospheres could affect radiation transport and thus in principle influence the overall radiative structure of these atmospheres. We have quantified the magnitude of these effects with simplified transmissivity models in a dynamic atmosphere, by assuming that linear bulk velocity gradients are present along otherwise homogeneous optical paths and by adopting Voigt line profile parameters appropriate for the radiatively forced regions of hot Jupiter atmospheres. We have found that bulk Doppler shifts systematically increase the equivalent widths of isolated radiative lines, relative to the equivalent widths in a static atmosphere, with excesses easily reaching several tens of percents for relevant model parameters.

Flux errors below the few percent level may well be acceptable in atmospheric models currently used to interpret the increasingly rich set of observational data on hot Jupiter atmospheres since other important atmospheric unknowns also contribute to modeling errors (e.g., the exact compositional profiles of radiatively active constituents). Flux errors at the level of several tens of percents or more may be too large to be ignored, however, especially if they originate from systematic excesses in the equivalent widths of important radiative lines. Given the link between line equivalent widths and radiative intensities discussed in §4.2 in the context of the narrow-band formalism, we therefore suggest that equivalent width excesses of the magnitude found in several of our idealized models could have a significant impact on radiative fluxes and the overall radiative energy balance of hot Jupiter atmospheres.

However, we must also caution that, beyond these preliminary arguments, it is not possible to settle this question without a considerably more detailed calculation than the one presented here. Indeed, it is the combined effect of bulk Doppler shifts on a vast number of radiative lines, all with varying degrees of optical thickness, weighted by the various Planck functions of the atmospheric layers under consideration (thus depending on the atmospheric temperature profile itself), along a variety of inhomogeneous optical paths, which ultimately determines by how much the overall radiative balance of the dynamic atmosphere is affected. By contrast, our simple transmissivity and equivalent width models were focused on single isolated lines with purely linear velocity gradients along arbitrary, homogeneous optical paths. Furthermore, contributions from continuum opacity sources in the atmosphere, for instance in cloudy regions, could reduce the impact of bulk Doppler shifts on the atmospheric radiation transport, since small shifts mostly affect narrow radiative lines. Various simplifying assumptions made in our models would thus be invalidated in a more realistic radiative transport calculation. Interestingly, the full radiation transport problem in a dynamic atmosphere may be amenable to practical numerical solutions in the future

(e.g., Knop et al. 2009).

It is also worth emphasizing that our discussion has largely focused on the long-wavelength (thermal) component of the atmospheric radiation spectrum, for which the diffuse approximation and the use of an isotropic (Planck) source function are justified. At first, one may be tempted to neglect the effects of bulk Doppler shifts from horizontal winds in the treatment of short-wavelength atmospheric radiation since the corresponding beam-like insolation is vertical in first approximation. This could be misleading, however. When scattering is important, as is usually the case, it generates optical paths slanted enough that they could become much more susceptible to the bulk Doppler shifts caused by horizontal winds. Furthermore, there is a significant fraction of the atmosphere that is located far enough away from the substellar point to be subject to partially slanted irradiation. In the case of close-in planets like hot Jupiters, the finite size of the stellar disk could also contribute to slanted irradiation and thus an increased sensitivity to Doppler shifts from horizontal winds. Let us emphasize that radiation transport in a dynamic atmosphere with an anisotropic source function, as would result from multiple scattering of the beam-like insolation in the short-wavelength portion of the atmospheric radiation spectrum, would lead to a considerably more complex formulation of the radiative transfer problem than discussed here for the case of diffuse thermal radiation (e.g., Eq. [2]). For example, one wonders whether the anisotropic transport resulting from atmospheric bulk motions could result in a stronger polarization signal than has been estimated on the basis of static radiative transfer calculations (e.g., Seager et al. 2000).

Interestingly, the various short-wavelength radiation transport effects mentioned above should be particularly pronounced in the context of transmission spectroscopic measurements, which specifically probe nearly horizontal optical paths at the atmospheric planetary limb during transits. Essentially all transit spectroscopic diagnostics could thus be affected by bulk Doppler shifts from fast atmospheric winds. Brown (2001) has presented a detailed discussion of this problem, including consequences of the vertical gradients of horizontal wind velocity. The possibly more important effects of bulk Doppler shifts along a specific optical path were omitted from these calculations, however, even though the author did comment on the expectation of increased line equivalent widths. It may thus prove important to carefully reassess various interpretations about the chemical composition of hot Jupiter atmospheres based on transit spectroscopic measurements with models which properly account for radiation transport in dynamic, rather than static, atmospheres.

Finally, let us conclude by mentioning a few possible extensions of this work to other classes of planetary atmospheres. It would seem that the standard static assumption for the treatment of radiation transport in Solar System planetary atmospheres is well justified.

Indeed, for these much cooler atmospheres, at a representative pressure level of 1 bar, radiative lines are significantly more pressure-broadened in Solar System atmospheres than in hot Jupiter atmospheres (see scalings in §3.2). In that limit, and for wind speeds well below the sound speed, our models do indicate very small excesses in the equivalent width of radiative lines.⁸ By contrast, the typically much hotter planets discovered by astronomers in recent years, which are often subject to unusually strong radiative forcing conditions, would seem to be more natural sites for the application of the radiation-hydrodynamical principles emphasized in the present work. Besides hot Jupiters, these principles could also find applications in the class of eccentric giant planets which experience transient atmospheric flash-heating during periastron passage (e.g., Langton & Laughlin 2008; Laughlin et al. 2009) and perhaps the emerging class of hot super-Earths, if the atmospheres of these planets are able to sustain wind velocities approaching or exceeding the sound speed in the presence of significant ground drag.

We thank Adam Burrows, Jeremy Goodman, Brad Hansen, Frits Paerels and Ed Spiegel for useful discussions and an anonymous referee for comments that helped improve the quality of this manuscript. This work was supported by the NASA OSS program, contract #NNG06GF55G, a NASA Graduate Student Research Program Fellowship, contract #NNX08AT35H, and the Spitzer Space Telescope Program, contract # JPLCIT 1366188. We also thank Drake Deming for supporting this work.

REFERENCES

- Agol, E., Cowan, N. B., Bushong, J., Knutson, H., Charbonneau, D., Deming, D., & Steffen, J. H. 2009, IAU Symposium, 253, 209
- Barman, T. S., Hauschildt, P. H. & Allard, F. 2005, ApJ, 632, 1132
- Brown, T. M. 2001, ApJ 553, 1006
- Buchler, J. R. 1983, Journal of Quantitative Spectroscopy and Radiative Transfer 30, 395
- Burkert, A., Lin, D. N. C., Bodenheimer, P. H., Jones, C. A., & Yorke, H. W. 2005, ApJ, 618, 512

⁸Interestingly, Neptune’s and Saturn’s upper atmospheres and their near-sonic wind speeds (e.g., Suomi et al. 1991; Li et al. 2008) may constitute a partial exception to this rule, despite cold atmospheric temperatures.

- Burrows, A., Budaj, J., & Hubeny, I. 2008, *ApJ*, 678, 1436
- Castor, J. I. 1970, *MNRAS* 149, 111
- Castor, J. I. 2004, *Radiation Hydrodynamics*. Cambridge, UK: Cambridge University Press
- Charbonneau, D., et al. 2005, *ApJ*, 626, 523
- Charbonneau, D., Brown, T. M., Noyes, R. W., & Gilliland, R. L. 2002, *ApJ*, 568, 377
- Charbonneau, D., Knutson, H. A., Barman, T., Allen, L. E., Mayor, M., Megeath, S. T., Queloz, D., & Udry, S. 2008, *ApJ*, 686, 1341
- Cho, J. Y.-K., Menou, K., Hansen, B. M. S., & Seager, S. 2003, *ApJ*, 587, L117
- Cho, J. Y.-K., Menou, K., Hansen, B. M. S., & Seager, S. 2008, *ApJ*, 675, 817
- Cooper, C. S., & Showman, A. P. 2005, *ApJ*, 629, L45 (C&S)
- Cooper, C. S., & Showman, A. P. 2006, *ApJ*, 649, 1048
- Cowan, N. B., Agol, E., & Charbonneau, D. 2007, *MNRAS*, 552
- Deming, D., Seager, S., Richardson, L. J., & Harrington, J. 2005, *Nature*, 434, 740
- Dobbs-Dixon, I., & Lin, D. N. C. 2008, *ApJ*, 673, 513
- Fortney, J. J., Cooper, C. S., Showman, A. P., Marley, M. S., & Freedman, R. S. 2006, *ApJ*, 652, 746
- Fortney, J. J., Lodders, K., Marley, M. S., & Freedman, R. S. 2008, *ApJ*, 678, 1419
- Freedman, R. S., Marley, M. S. & Lodders, K. 2008, *ApJS* 174, 504
- Goody, R. M. & Yung, Y. L. 1989, *Atmospheric radiation : theoretical basis*. 2nd ed., New York, NY: Oxford University Press
- Grillmair, C. J., Charbonneau, D., Burrows, A., Armus, L., Stauffer, J., Meadows, V., Van Cleve, J., & Levine, D. 2007, *ApJ*, 658, L115
- Guillot, T., & Showman, A. P. 2002, *A&A*, 385, 156
- Harrington, J. et al. 2006, *Science*, 314, 623
- Harrington, J., Luszcz, S., Seager, S., Deming, D., & Richardson, L. J. 2007, *Nature*, 447, 691

- Hsieh, S.-H. & Spiegel, E. A. 1976, *ApJ* 207, 244
- Iro, N., Bezdard, B. & Guillot, T 2005, *A&A*, 436, 719
- Knop, S., Hauschildt, P. H. & Baron, E. 2009, *A&A* 496, 295
- Knutson, H. A., et al. 2007, *Nature*, 447, 183
- Knutson, H. A., et al. 2009a, *ApJ*, 690, 822
- Knutson, H. A., Charbonneau, D., Allen, L. E., Burrows, A., & Megeath, S. T. 2008, *ApJ*, 673, 526
- Knutson, H. A., Charbonneau, D., Burrows, A., O’Donovan, F. T., & Mandushev, G. 2009b, *ApJ*, 691, 866
- Langton, J., & Laughlin, G. 2007, *ApJ*, 657, L113
- Langton, J., & Laughlin, G. 2008, *ApJ*, 674, 1106
- Laughlin, G. et al. 2009, *Nature* 457, 562
- Li, L. et al. 2008, *Geo. Res. Lett.* 35, L23208
- Liou, K. N. 2002, *An introduction to atmospheric radiation*, 2nd Ed. New York, NY: Academic Press
- Machalek, P., McCullough, P. R., Burke, C. J., Valenti, J. A., Burrows, A., & Hora, J. L. 2008, *ApJ*, 684, 1427
- Menou, K., & Rauscher, E. 2008, *ApJ* 700, 887
- Mihalas, D. & Mihalas, B. W. 1984, *Foundations of radiation hydrodynamics*. New York: Oxford University Press.
- Pont, F., Knutson, H., Gilliland, R. L., Moutou, C., & Charbonneau, D. 2008, *MNRAS*, 385, 109
- Rauscher, E. & Menou, K. 2009, arXiv:0907.2692, *ApJ* submitted
- Richardson, L. J., Deming, D., Horning, K., Seager, S., & Harrington, J. 2007, *Nature*, 445, 892
- Rodgers, C. D. & Walshaw, C. D. 1966, *Quarterly Journal of the Royal Meteorological Society* 92, 67

- Rybicki, G. B. 1970, in *Spectrum Formation in Stars with Steady-State Extended Atmospheres*, Proceedings of IAU Colloq. 2, Eds H. G. Groth and P. Wellmann. National Bureau of Standards Special Publication 332., p.87
- Rybicki, G. B. & Hummer, D. G. 1978, *ApJ* 219, 654
- Seager, S., Richardson, L. J., Hansen, B. M. S., Menou, K., Cho, J. Y.-K., & Deming, D. 2005, *ApJ*, 632, 1122
- Seager, S., Sasselov, D.D., 1998, *ApJ*, 502, L157
- Seager, S., Whitney, B. A. & Sasselov, D. D. 2000, *ApJ* 540, 504
- Sharp, C. M. & Burrows, A. 2007, *ApJS* 168, 140
- Showman, A. P., Cooper, C. S., Fortney, J. J., & Marley, M. S. 2008a, *ApJ*, 682, 559
- Showman, A. P., Fortney, J. J., Lian, Y., Marley, M. S., Freedman, R. S., Knutson, H. A., & Charbonneau, D. 2009, *ApJ*, 699, 564
- Showman, A. P. & Guillot, T. 2002, *A&A*, 385, 166
- Showman, A. P., Menou, K., & Cho, J. Y.-K. 2008b, *Astronomical Society of the Pacific Conference Series*, 398, 419
- Showman, A. P., Cho, J. Y.-K. & Menou, K. 2010, in *Exoplanets*, ed. S. Seager, arXiv:0911.3170
- Sing, D. K., Vidal-Madjar, A., Lecavelier des Etangs, A., Désert, J.-M., Ballester, G., & Ehrenreich, D. 2008, *ApJ*, 686, 667
- Sudarsky, D., Burrows, A. & Pinto, P. 2000, *ApJ*, 538, 885
- Suomi, V. E., Limaye, S. S. & Johnson, D. R. 1991, *Science* 251, 929
- Swain, M. R., Bouwman, J., Akeson, R. L., Lawler, S., & Beichman, C. A. 2008a, *ApJ*, 674, 482
- Swain, M. R., Vasisht, G., & Tinetti, G. 2008b, *Nature*, 452, 329
- Tinetti, G., et al. 2007, *Nature*, 448, 169
- Thomas, G. E. & Stamnes, K. 2002, *Radiative Transfer in the Atmosphere and Ocean*. Cambridge, UK: Cambridge University Press

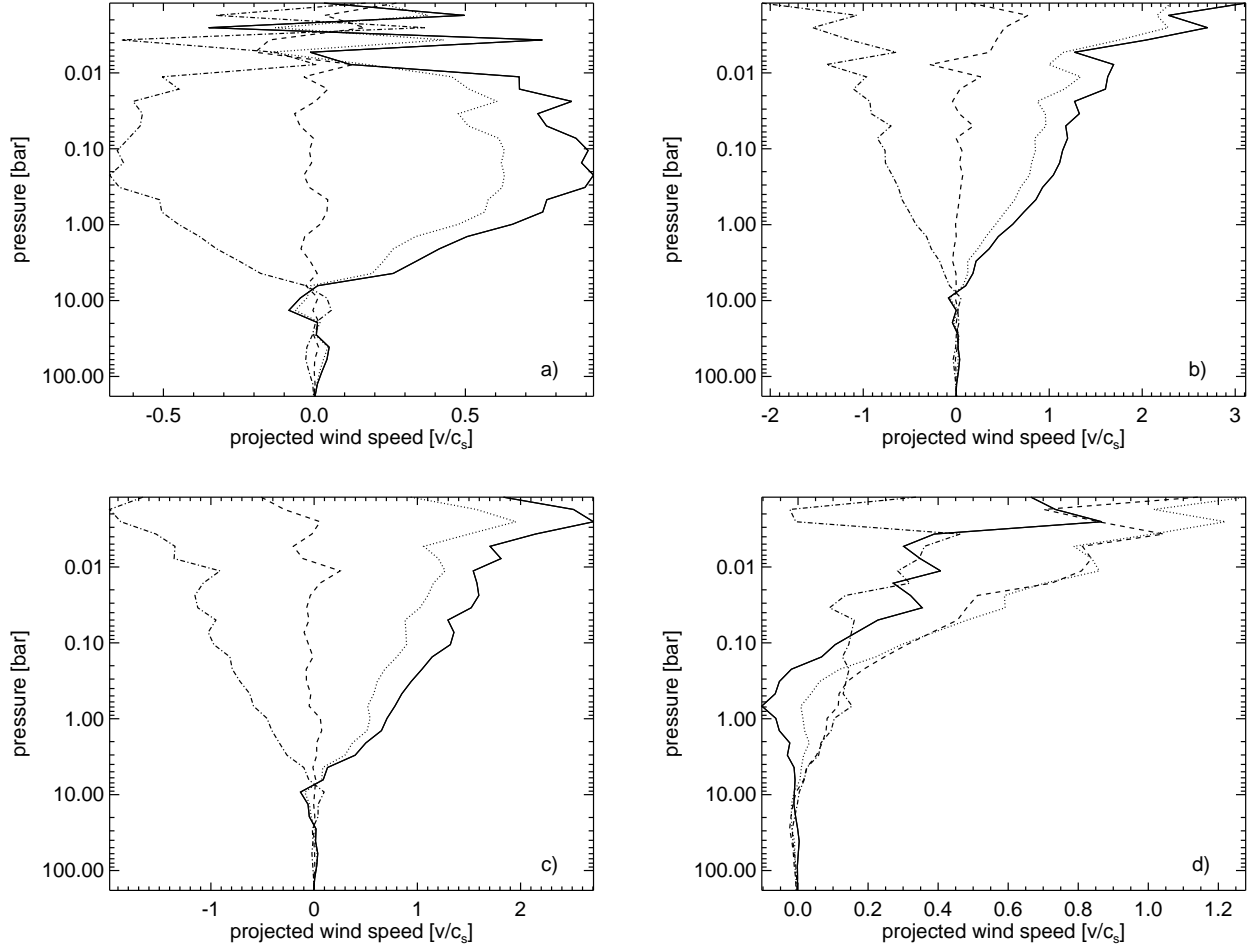


Fig. 1.— Representative profiles of wind velocities, in units of the local sound speed c_s , projected along various optical paths at a fixed zenith angle $\theta_0 = 53$ degrees in the atmospheric circulation model of Rauscher & Menou (2009). The various panels show profiles at the model substellar point (a), antistellar point (b), west equatorial terminator (c) and north pole (d). In each panel, the various curves show projected velocity profiles for optical paths oriented to the east (solid line), north-east (dotted), north (dashed) and north-west (dash-dotted). Velocity differentials which are a sizable fraction of, and in some cases exceed, c_s are typical.

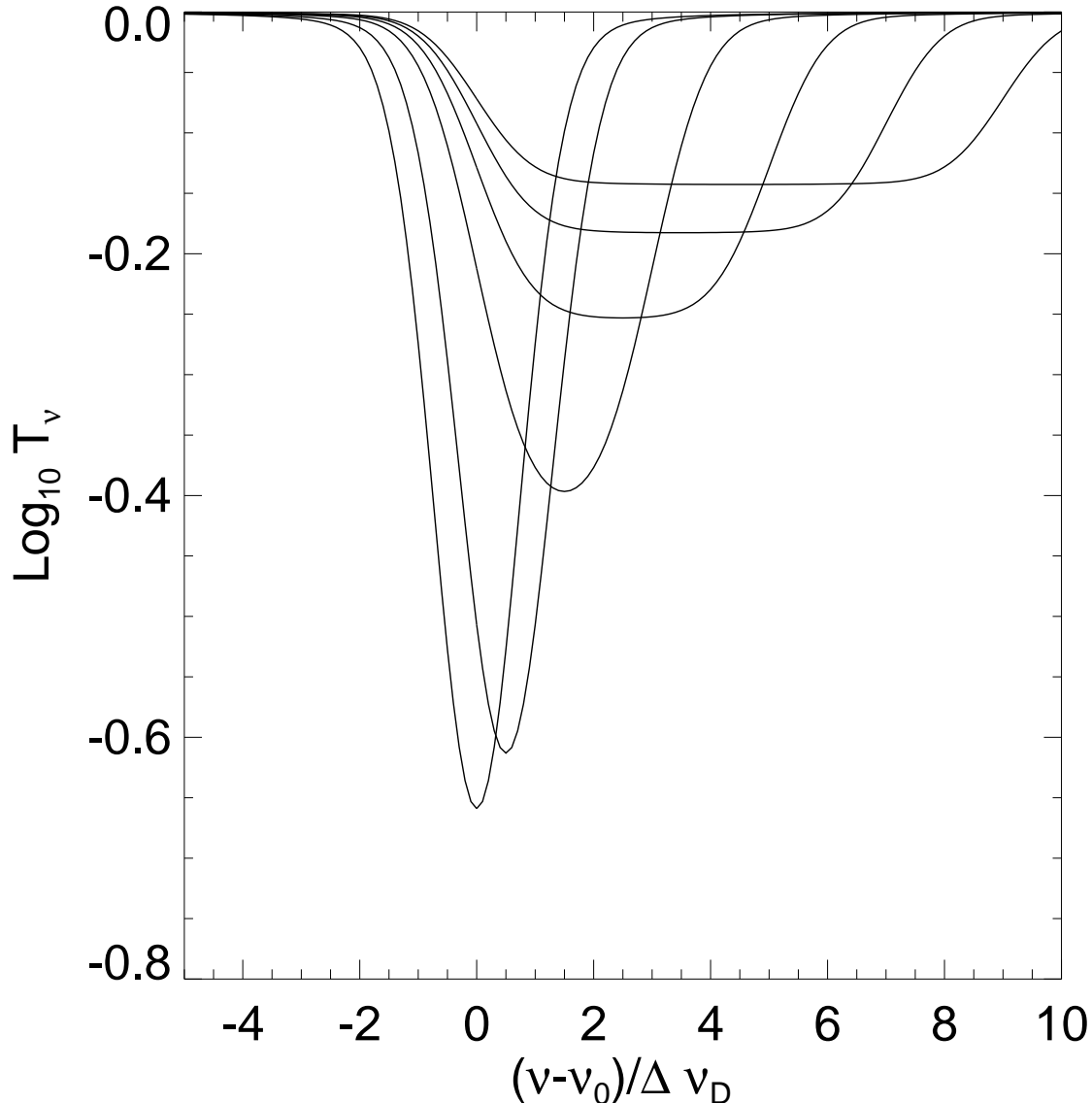


Fig. 2.— Monochromatic transmissivity curves for a line centered at $\nu = \nu_0$ with a Voigt profile shape and a fixed ratio of Doppler- to pressure-broadening widths, $\Delta\nu_D/\Delta\nu_p = 10$. From left to right, transmissivity profiles are shown for linear bulk velocity gradients with total offsets $V_{\text{proj}}/\Delta\nu_D = 0$ (static), 1, 3, 5, 7 and $9 \times c/\nu_0$ over the full optical path. The specific model shown here is marginally optically-thick, with a line-integrated absorption coefficient $\tilde{k}_{\text{tot}} = 3$ over the full optical path, but these transmissivity profiles are representative of more general cases. Monochromatic transmissivities are significantly affected by bulk Doppler shifts in excess of a few thermal Doppler widths. The increasingly blue-shifted transmissivity profiles shown have equivalent widths exceeding that of the static profile by 2.4, 14, 24, 31 and 35%, from left to right.

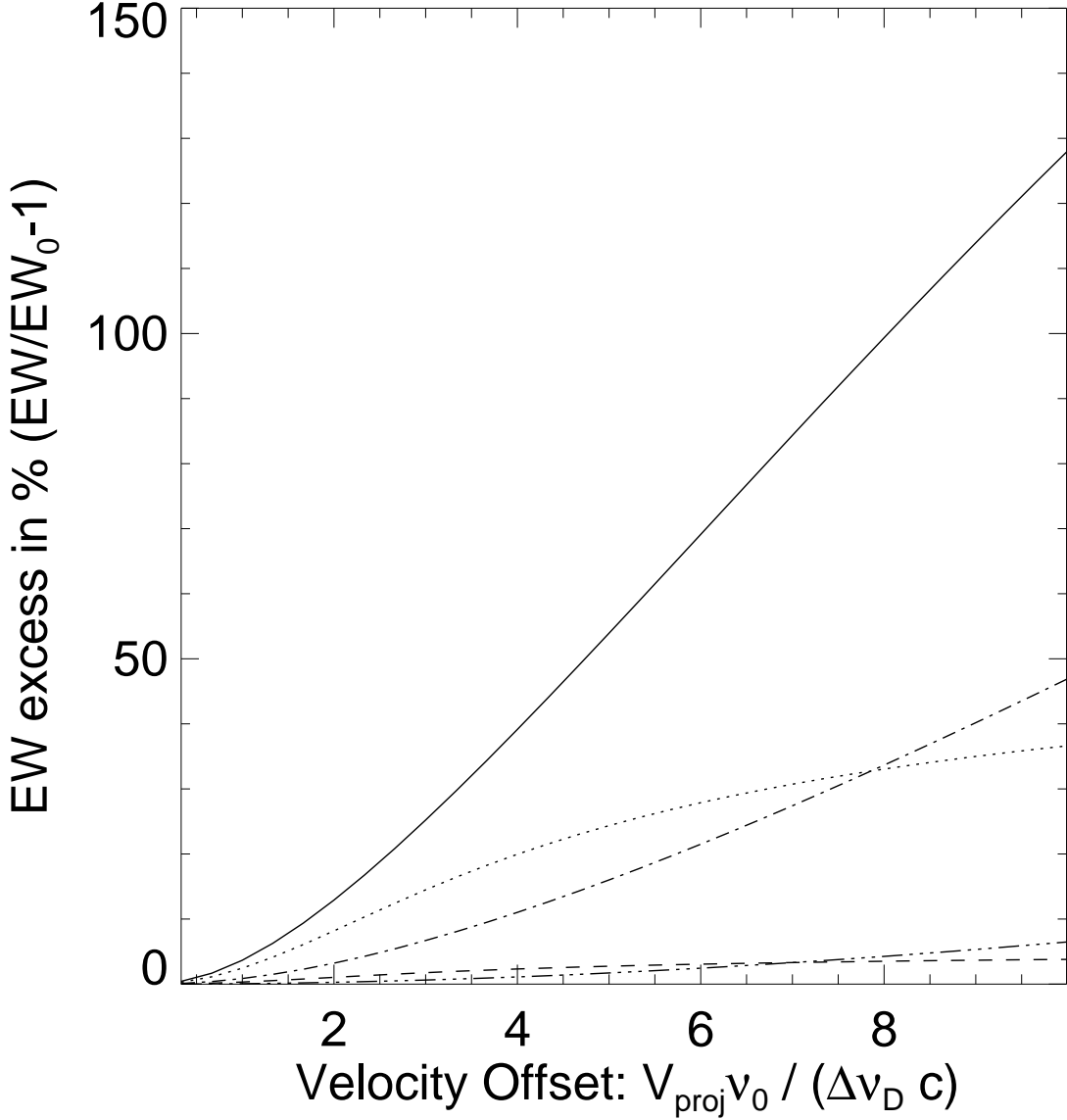


Fig. 3.— Equivalent width excess (in %) of a radiative line in a dynamic atmosphere with a linear bulk velocity gradient, as a function of V_{proj} , the total velocity offset over the optical path, in units of the line’s thermal Doppler width ($\Delta\nu_D \times c/\nu_0$). In this specific model, the line has a Voigt profile shape with a fixed ratio of Doppler- to pressure-broadening widths, $\Delta\nu_D/\Delta\nu_p = 10$. The various curves show results for lines with different total absorption coefficients: $\tilde{k}_{\text{tot}} = 0.3$ (dashed line), 3 (dotted), 30 (solid), 300 (dash-dotted) and 3000 (triple-dot dashed).

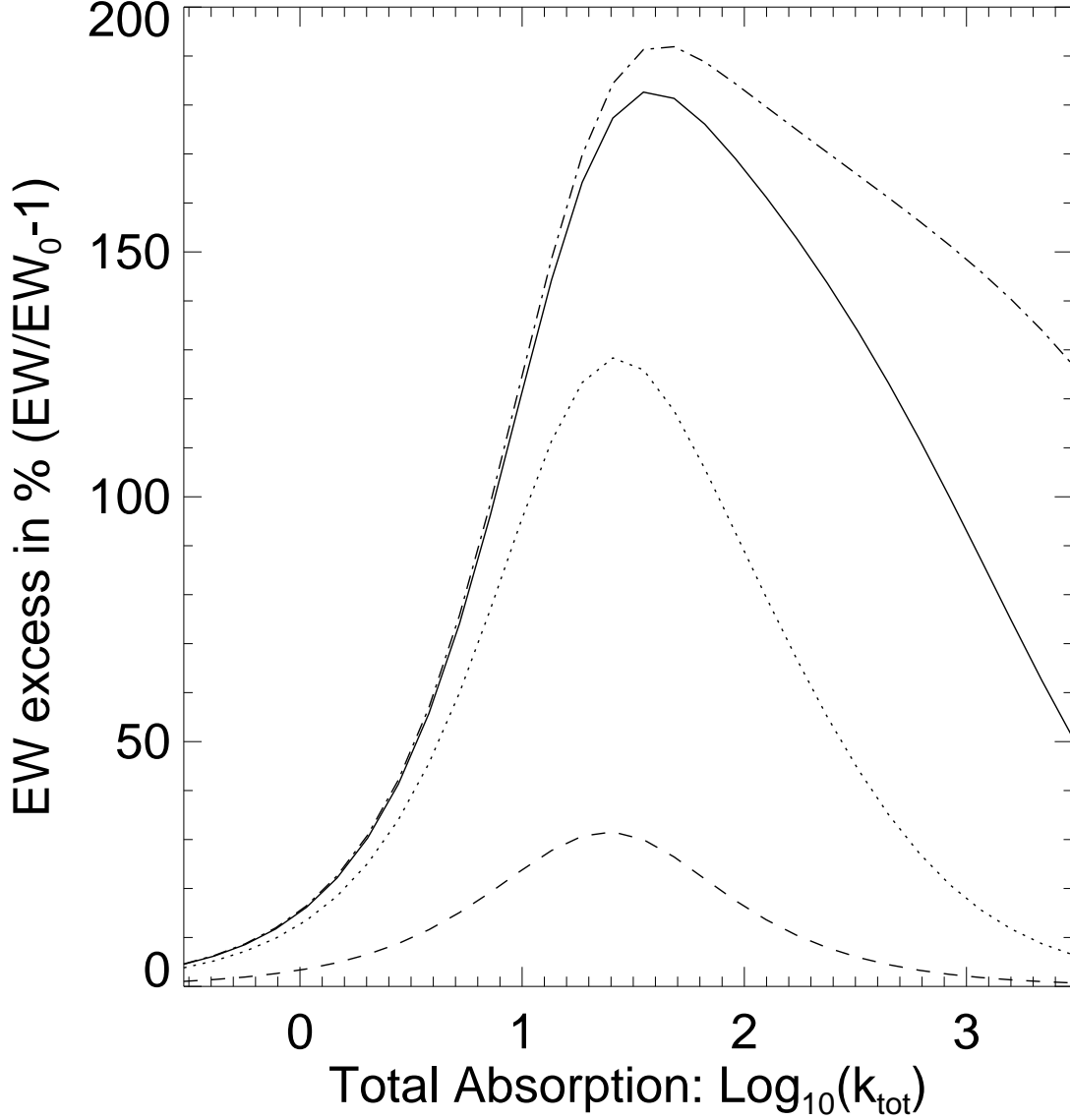


Fig. 4.— Equivalent width excess (in %) of a radiative line in a dynamic atmosphere with a linear bulk velocity gradient, as a function of the total line absorption coefficient, \tilde{k}_{tot} . In this specific model, a relatively large value of the total velocity offset over the full optical path, $V_{\text{proj}} = 10 \Delta\nu_D \times c/\nu_0$, is adopted. The line has a Voigt profile shape and the various curves shown correspond to different ratios of the Doppler- to pressure-broadening widths: $\Delta\nu_D/\Delta\nu_p = 1$ (dashed line), 10 (dotted), 100 (solid) and 1000 (dash-dotted).